J Nanostruct 15(4): 1626-1641, Autumn 2025

RESEARCH PAPER

# Antibacterial and Anti-Biofilm Efficacy of Novel Nisin-Loaded Silver Nanoparticles Biosynthesized by *Fusarium Solani* Against Clinical Pathogens

***Asia Salih, Mohammed Hamk****

*Medical Laboratory Science Department, College of Science, , Charmo University, Sulaymaniyah, Chamchamal, Iraq*

**ARTICLE INFO**

***Article History:***
*Received 11 June 2025*
*Accepted 10 August 2025*
*Published 01 October 2025*

***Keywords:***
*Anti-Biofilm*
*Antibacterial*
*Biosynthesis*
*Fusarium solani*
*Nisin-Loaded Silver Nanoparticles*

**ABSTRACT**

Currently, nanoparticles, particularly silver nanoparticles, are interesting because of their unique physicochemical attributes and extensive range of biological, catalytic, electrical, and environmental applications. Among various fabrication methods, green synthesis presents an eco-friendlier and more sustainable alternative compared to traditional chemical or physical techniques. This study explores the green synthesis of silver nanoparticles employing the cell-free supernatant derived from Fusarium solani, and the bioconjugation of silver nanoparticles with an antimicrobial peptide nisin was evaluated in a one-pot reaction. The synthesis conditions have been optimized for high yield and favorable nanoparticle characteristics. The optimization results were 9.0 and 72 h for in 1:2 v/v (cell-free supernatant: salt), 1.5 mM of salt. The synthesized nanoparticles were characterized using ultraviolet-visible spectroscopy, transmission electron microscopy, scanning electron microscopy, x-ray diffraction, Fourier transform infrared spectroscopy, energy dispersive x-ray spectroscopy, atomic force microscopy, and zeta potential studies to verify the formation of nanoparticles. Characterization averaged particle sizes of 10.7 nm for silver nanoparticles and 12.8 nm for nisin-loaded silver nanoparticles were found to be quasi-spherical. Both nanoparticles exhibited potent antimicrobial behavior, indicating their potential against pathogenic bacteria. This work emphasizes the efficacy of green-synthesized silver nanoparticles and their nisin-conjugated analogues as effective, low-cost, and environmentally friendly biomedical agents, especially in antimicrobial treatment as well as eliminating biofilms.

**How to cite this article**
*Salih A., Hamk M. Antibacterial and Anti-Biofilm Efficacy of Novel Nisin-Loaded Silver Nanoparticles Biosynthesized by Fusarium Solani Against Clinical Pathogens. J Nanostruct, 2025; 15(4):1626-1641. DOI: 10.22052/JNS.2025.04.012*

## INTRODUCTION

Antibiotic resistance is considered one of the most critical worldwide threats to humanity in the 21st century. Reducing the effectiveness of antimicrobial treatments has created a need for novel designs and the development of antibacterial agents [1] . However, the improper use and excessive intake of antibiotics increase the development of antibacterial resistance which allows pathogenic bacteria to create drug-

* *Corresponding Author Email: mohammed.hamk@chu.edu.iq*

resistant [2]. One of the key factors leading to antimicrobial resistance (AMR) is bacterial biofilm formation, which supplies the pathogens with a protective shield against antibiotics. In reality, Biofilm development is another method that bacteria might use to survive when antibiotics are present [3]. According to reports from the National Institutes of Health (NIH), microbiological biofilm is responsible for about 65 % of microbiological infections and 80 % of chronic infections, respectively [4].

Although scientists, pharmacists, and doctors search for safe, broad-spectrum medications, resistant and biofilm-forming bacteria remain difficult to treat. Due to these issues, nanotechnology and nanoparticles as antibiotic alternatives seem appealing. Silver nanoparticles (AgNPs) are intriguing nanomaterials because of their distinctive properties and several nanomedicine applications. AgNPs release and quantity determine silver's antibacterial properties. Non-ionized silver binds to tissue proteins and damages bacterial cell walls and nuclear membranes. Nanoparticles of silver denature and limit bacterial growth by binding DNA and RNA [5,6]. Consequently, AgNPs can be synthesized through different methods, including biological, physical, and chemical. Among these, biological synthesis is regarded as a sustainable and environmentally friendly approach, as it reduces the reliance on toxic chemicals [7]. Moreover, fungal AgNPs can be efficiently synthesized using species from the genus *Fusarium*, which are favored due to their filamentous morphology and ease of isolation from plant and soil sources. This well-characterized genus grows on simple media at moderate temperatures, making it ideal for nanoparticle biosynthesis [8].

Recent developments in nanoparticle functionalization have brought attention to the advantages of peptide-conjugated AgNPs, which extend beyond fungal-mediated production. Both nisin-loaded silver nanoparticles (N-AgNPs) and tryasine-conjugated AgNPs exhibited strong activity against both Gram-positive and Gram-negative bacteria, including *Staphylococcus aureus*, methicillin-resistant Staphylococcus aureus (MRSA), and *Escherichia coli*. This suggests that conjugation enhances targeting efficiency by increasing the local concentration of the active agent at the infection site [8-10].

Building on these advances and enhancing the robustness of AgNPs against multidrug-resistant pathogens, incorporating safe antimicrobial agents such as the peptide nisin onto AgNPs represents a promising strategy to improve therapeutic efficacy. Nisin is a polycyclic peptide that functions as an antimicrobial agent and contains 34 amino acid residues with five lanthionine rings [11]. Nisin is a cationic bacteriocin that comes from Lactococcus lactis and is safe to use (GRAS). It was initially employed to keep food fresh, but its ability to kill Gram-positive microorganisms has made it useful in medicine as well [12,13]. The mechanism of the action of the antibacterial nisin is mainly due to the interaction with the negatively charged cytoplasmic membrane and the formation of pores on cell membranes, which results in the alteration of the permeability of the cells [14].To our knowledge, no studies have reported the use of Fusarium species to synthesize nisin-functionalized AgNPs. While Fusarium-derived AgNPs are known for their antimicrobial activity, their conjugation with peptides like nisin remains unexplored, representing a novel and promising research direction. This study aimed to biosynthesize, optimize, and characterize AgNPs. AgNPs using the filamentous fungus *Fusarium solani*. The resulting AgNPs were then conjugated with nisin to produce N-AgNPs. These nanomaterials were subsequently evaluated for their synergistic antibacterial efficacy and antibiofilm activity.

## MATERIALS AND METHODS

### *Materials*

Bacterial growth was done on Nutrient Broth (NB) and Luria-Bertani (LB) broth, while Mueller-Hinton Broth (MHB) was used for testing for antibacterial sensitivity. Fungi were cultivated in Potato Dextrose Broth (PDB). Media were sterilized by autoclaving at 121°C for 15 min and made up according to standard methods. The nisin was obtained from Smart Kimya (Izmir/ Turkey). All the reagents used were analytical grade.

### *Optimization of silver nanoparticles*

The optimization of AgNPs production was achieved by methodically assessing four critical elements influencing synthesis yield. Their parameters were utilized to optimize nanoparticle creation and enhance production efficiency. This variable includes the $AgNO_3$ salt concentration (0.5, 1, and 1.5 mM), the reduction time (24, 48, and 72 h), the pH value (5.0, 7.0, and 9.0), and

the volume ratio of cell-free supernatant (CS-F) to $AgNO_3$ (1:1, 1:2, and 2:1 V/V). Every experiment was carried out in triplicate to confirm the dependability and reproducibility.

*Optimization of nisin-loaded biosynthesized AgNPs*

To enhance stability and antibacterial efficacy, the nisin was loaded onto synthesized AgNPs by adjusting critical formulation conditions. Different concentrations (0.5, 1, and 3 mg/ml) were introduced to the biosynthesized AgNPs, after which the solution was subjected to a shaker incubator for an additional hour at 120 rpm to enhance homogeneous binding to the AgNPs.

*Characterization of nanoparticles*

Optical absorption spectra were obtained with a UV-line 9400 (SI Analytics) system. The samples were scanned from 300 to 600 nm to preliminarily characterize reduced AgNPs and N-AgNPs. Transmission electron microscopy (TEM) Ultrahigh-resolution TEM can visualize NPs at the nanoscale and their components. This method helps to explain membrane construction, development, and fouling [15]. The morphology of nano-structural materials is typically examined using scanning electron microscopy (SEM), as well as analysis of size, shape, purity, surface morphology, and dispersion for biosynthesized nanoparticles [16]. Under high vacuum mode, 4.83 mm working distance images were taken with numerous magnifications. The elemental compositions of NPs were investigated by energy dispersive X-ray spectroscopy (EDS) (1024 channels, 20 kV, 10 nA, 12,500× magnification). The crystallographic structure of materials is characterized using X-ray diffraction (XRD), the chemical composition and physical features of the material, and the NP thin film [17]. The average crystalline size of NPs was estimated using Debye-Scherrer's equation based on the full width at half maximum (FWHM) value of the peaks [18]. Nanoscale surface analysis is safe with high-resolution atomic force microscopy (AFM). We produce air, liquid, or vacuum 3D topography. Sharp-tip, flexible-cantilever AFM probe. Interatomic cantilever deflections are measured by lasers. Movements offer nanometer-resolved 3D Surface Images [19]. the functional groups of materials were identified by analyzing certain peaks using the Fourier transform infrared spectroscopy (FTIR) technique. KBr-ground powdered samples were scanned for the spectrum between 400 to 4000 $cm^{-1}$ and resolution to 4 $cm^{-1}$ [20]. The Zeta potential assay was used for measuring the charge and stability of NPs. The particles above ±30 mV exhibit high electrostatic stability, while lower values may stabilize sterically [21]. The zeta potential of samples was assessed at 25°C using standard settings in a dispersion medium.

*Isolation and molecular identification of pathogenic bacteria*

*Isolation of pathogenic bacteria*

Urine, ear, and wound swabs were used to isolate pathogenic bacteria, including *Escherichia coli, Acinetobacter baumannii,* and *Staphylococcus aureus*. Identification was performed using molecular techniques and the BD Phoenix™ technology. One single colony for each isolate was chosen and kept in glycerol stock at –20°C for additional study.

*Identification of bacteria by BD Phoenix™*

BD Phoenix is an automated microbiology system (BD Diagnostic Systems) used for the identification (ID) and antimicrobial susceptibility testing (AST) [22]. Results led isolates to be categorized as sensitive, resistant, or multidrug-resistant (MDR).

*Molecular identification of pathogenic bacteria*

The polymerase chain reaction (PCR) technique was employed for the molecular identification of isolated Bacteria, which is a technique used to amplify a specific sequence of DNA through denaturation, annealing, and extension steps. The bacterial total genome was extracted using a (for better BIO-TECH) following the manufacturer's guidelines. The PCR reaction was carried out in a total volume of 20 µl, including 10 µl master mix (BIO-Rada), 0.5 µl of each forward and reverse primers, 1µl of DNA template, and 8µl of DDH2O. The 16S rRNA gene was targeted using universal primers (7F:5'-AGAGTTTGATYMTGGCTCAG-3'), (1510R:5'ACGGYTACCTTGTTACGACTT-3') [23,24]. The PCR conditions were set to 30 cycles, with initial denaturation at 94°C for 5 minutes. Followed by denaturation at 94°C for 30 seconds, annealing at 58°C for 30 seconds, and extension at 72°C for 1 minute, with the final extension at 72°C for 5 minutes. Sanger DNA sequencing at Macrogen-Republic of Korea sequenced the ~1.5 kbp PCR product. Chromas software version 2.6.6 was used

for quality and sequencing edition (Technelysium).

*Construction of the phylogenetic trees*

Based on its 16S rRNA gene sequence, as previously reported, the isolate was taxonomically characterized by building a phylogenetic tree [25]. ClustalX 2.1 helped the sequence match closely related NCBI species [26]. Using MEGA 7, the phylogenetic tree was generated via the Neighbor-joining method, applying (Kimura 2-parameter model, with 1000 bootstrap repetitions. [27].

*Antibacterial activity assay*

A disc diffusion assay was done according to [28]. with some modifications. The bacteria were activated in Müller-Hinton broth (MHB) at 37°C for 22–24 h. Then, 100 µl culture broth (0.5 McFarland) was uniformly distributed on Müller-Hinton agar plates. Different concentrations (4, 3, 2, and 1, 2, 3, and 4 mg/ml) of AgNPs and N-AgNPs were prepared, a sterile filter paper discs (5mm diameter) were loaded with 50 µl of each prepared distinct concentration. The plates were incubated at 37°C for 18–22 hours to allow interaction between the bacteria and the nanoparticles. Additionally, nisin alone(0.5mg/ml) was added to a sterile disc under the same conditions to evaluate individual antibacterial activity. The inhibition zones were daily measured in triplicate.

To calculate the minimum inhibitory concentration (MIC) for AgNPs and Nisin-AgNPs, Pathogenic bacterial isolates were adjusted to ($10^8$cells/mL), equivalent to 0.5 McFarland, in fresh overnight cultures. A 120 µl bacterial culture was suspended in 96-well sterile polystyrene microtiter plates. Following this, 80 µl of AgNPs and N-AgNPs at the appropriate concentrations (0.06, 0.125, 0.25, 0.75, 0.5, and 1 mg/ml) were introduced. A 120 µl of bacteria, 80 µl of media used as a positive control, AgNPs, N-AgNPs, and medium as a blank were added. incubated overnight at a shaker incubator, and a microplate reader assessed each well's absorbance at 600 nm (BioTek (ELx800) / USA) [20].

*Biofilm Inhibition Assay*

Bacteria were cultured in LB medium for 24 h to inhibit biofilm formation by AgNPs and N-AgNPs. After adjusting to ($10^8$cells/mL), equivalent to 0.5 McFarland, each 96-well plate was filled with 120 µl of bacterial suspension and 80 µl of AgNPs and N-AgNPs at various concentrations (0.06, 0.125, 0.25, 0.5, 1mg/ml). After incubation for 24 h, all wells were discarded and dried for 15 min. Each well was then filled with 200 µl of deionized water, left for 2 min, discarded, and allowed to dry in the room for 30 min. Then, each well was treated with 200 µl of 0.1% crystal violet and left at room temperature for 15–20 min. the stains were then removed, and each well was washed three times with deionized water, and air-dried for an hour. followed by adding 200 µl of absolute ethanol and incubated for 15 min. A microplate reader is used to measure the absorbance at 595 nm [29].

*Statistical analysis*

All statistical analyses were conducted with IBM SPSS Statistics 27.0.1. All results are presented as the mean ± standard deviation (SD) and were conducted in triplicate. Using the Duncan post hoc test and one-way ANOVA, the significance of differences between the control and treated groups was ascertained as follows. Significance was determined by a p-value of $<0.05$.

**RESULTS AND DISCUSSION**

*Biosynthesis and optimization of silver nanoparticles*

The extracellular synthesis of NPs and the mechanism are still in question; the supernatant and its content of reductase enzymes are mainly responsible for the biosynthesis of NPs. In this study, during biosynthesis of AgNPs, precursor salt ($AgNO_3$) was reduced into AgNPs by *F. solani* supernatant. The preliminary characterization of AgNPs was done by their changing color after 1 h. of mixing the CF-S and $AgNO_3$ by UV–vis spectroscopy. The reduction of Ag+ into Ag0 was indicated by the color intensity, which transitioned from mild yellow to brown and ultimately to dark brown after 72 hours of incubation. The broad and durable surface plasmon resonance peak (SPR) at 414 nm suggests that the reaction state has undergone a change. A previous study has examined the production of AgNPs using *F. solani*, and the peak at 415 nm is nearly identical [30]. $AgNO_3$ concentration, pH, time, and ratio directly affect AgNP generation, as measured by UV-vis spectroscopy. The optimal conditions for synthesizing AgNPs using CS-F are pH 9, $AgNO_3$ concentration 1.5 mM, time after 72 h, ratio 1:2, as shown in Fig. 1. The optimal pH for AgNPs synthesis can vary depending on the type of microbe used. In this study, pH 9.0 was found

to be the most favorable, showing the highest absorbance and a sharp peak at 414 nm, and the color started to change within a few hours. The bioactive metabolites present in the fungal supernatant appear to be more stable and exhibit greater catalytic activity under alkaline conditions. In contrast, acidic pH levels led to aggregation of the AgNPs, while at pH 7.0 the synthesis was significantly reduced. The other study documented that the AgNPs were synthesized using *Fusarium exosporium,* which has the greatest production at pH 9.0 and pH 11 [31]. $AgNO_3$ concentration plays another key role in nanoparticle synthesis. In this study, 1.5 mM $AgNO_3$ was found effective for forming stable AgNPs. Higher concentrations can increase yield but may lead to particle aggregation, while lower levels may reduce efficiency. A similar result was reported by [32]. The authors showed that 1–2 mM $AgNO_3$ was the optimal concentration of salt for the formation of nanoparticles by fungal extracts. Time is a critical factor influencing the efficiency and yield of AgNPs synthesis. In this study, the reaction was monitored over a period of 24 to 72 h. A noticeable color change from pale yellow to dark brown indicated ongoing reduction of silver ions by fungal metabolites. UV-Vis spectroscopic analysis revealed that absorbance intensity gradually increased with time, reaching its peak at 72 h. suggesting continuous and efficient formation of nanoparticles. This implies that extending the reaction time allows for a more complete reduction of $Ag^+$ to $Ag^o$, leading to higher nanoparticle yield and stability [33]. These findings are consistent with previous reports, where prolonged incubation enhanced nanoparticle formation due to sustained activity of the reducing agents in the biological extract. A similar result was also reported in [34]. where maximum absorbance and nanoparticle formation were observed after 72 h. supporting the outcomes of this study.

The ratio between fungal supernatant and $AgNO_3$ plays a key role in nanoparticle formation. An appropriate ratio ensures efficient reduction

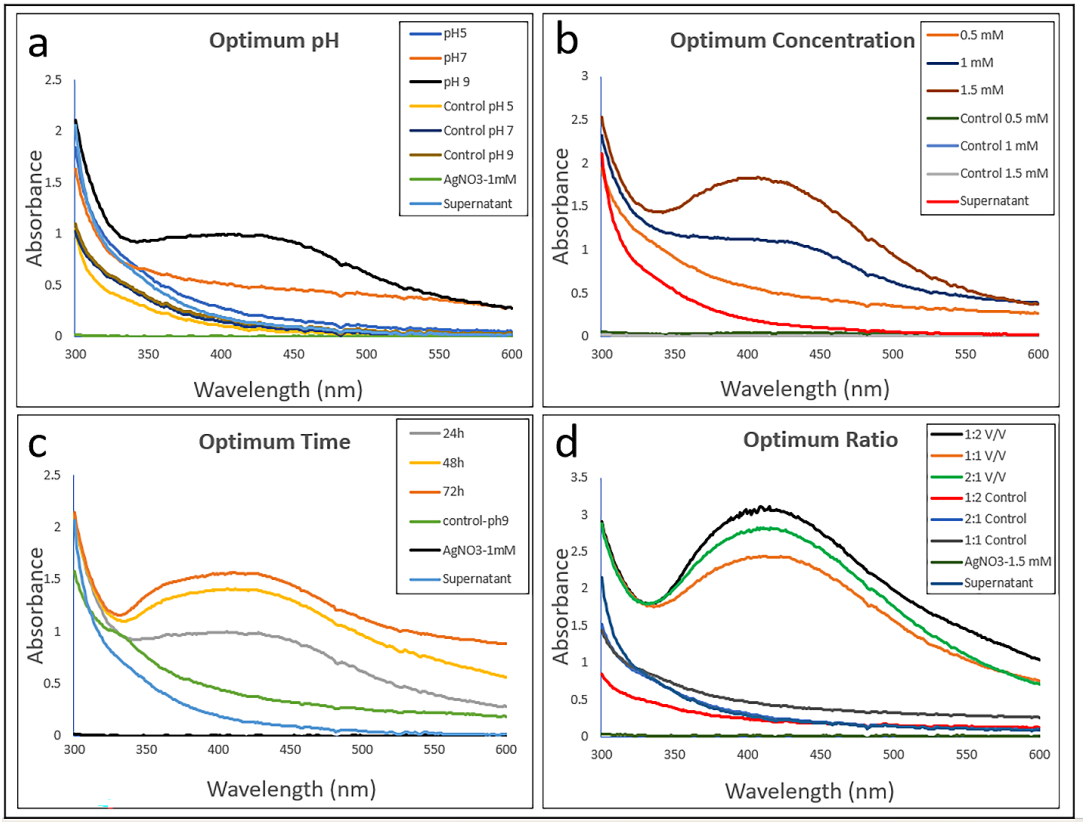


Fig. 1. The UV-vis absorption spectrum of AgNPs was synthesized by reducing silver ions and *F. solani* supernatant under different conditions: (a) pH, (b) salt concentration, (c) time, and (d) ratio

of $Ag^+$ ions and stable nanoparticle formation. In this study, a 1:2 ratio (supernatant to $AgNO_3$) produced the best results, leading to strong color change and maximum absorbance. Too little supernatant may limit reduction, while too much may cause aggregation or unstable particles. The ratio of fungal supernatant to silver nitrate is crucial for efficient AgNP synthesis. In this study, a 1:2 ratio gave optimal results. This ratio has also been suggested in previous studies. For instance, *F. solani* has been found to synthesize AgNPs stably with an optimum ratio of 1:1 or 1:2, and the resulting SPR peaks were about 414 - 420 nm, revealing the formation of NP efficiently [35,36].

*Nisin loaded onto biosynthesized AgNPs*

The synthesis of N-AgNPs was performed using different concentrations of nisin, and the color change was monitored over time. Nisin was effectively loaded into AgNPs to create and improve N-AgNPs by using various amounts and incubation times. Nisin was mixed into AgNPs at a concentration of 0.5 mg/ml (as the optimum concentration) after 72 h. of production, and then the mixture was shaken for one more hour. Fig. 2 shows the formation of N-AgNPs. Loading nisin onto AgNPs resulted in a slight red shift of the UV-Vis absorption peak from 414 nm to 417 nm, indicating successful interaction or binding between nisin and the nanoparticle surface. This shift suggests a change in the SPR due to nisin coating. N-AgNPs also showed enhanced antimicrobial activity compared to AgNPs alone, due to the synergistic effect of silver and nisin. Similar findings were reported by [37]. where nisin-functionalized nanoparticles exhibited efficacy against *Pseudomonas aeruginosa.*

*Characterization of nanoparticles*

The conversion of $AgNO_3$ and fungal cell-free supernatant into AgNPs was evidenced by UV-Vis spectroscopy, as indicated previously in (Fig. 1) and a noticeable color change from light yellow to dark brown. This visual change is often attributed to the SPR of AgNPs, as shown previously in (Fig. 2b), which has been extensively reported in biosynthesis studies [38,39]. reported that a color change is initial evidence of nanoparticle formation. Similarly [40]. reported the formation of brown color during AgNP formation by *Fusarium oxysporum* and the reduction of silver metal to Ag0 [41] highlighted this as a common confounding parameter in plant vs. micro pathogen-mediated NP synthesis. Such results corroborate the present observation and establish the color change as a reliable indicator of AgNP synthesis.

TEM results show that the AgNPs had mostly spherical to quasi-spherical shapes for AgNPs and quasi-spherical shapes for N-AgNPs. The particle sizes of AgNPs range from around 6.4 nm to 17 nm (Fig. 3A-a). The average particle size computed was 10.7 nm. Such shapes and nanoscale sizes match those of usual biosynthesis-produced AgNPs [42,43]. With a rather limited distribution, as

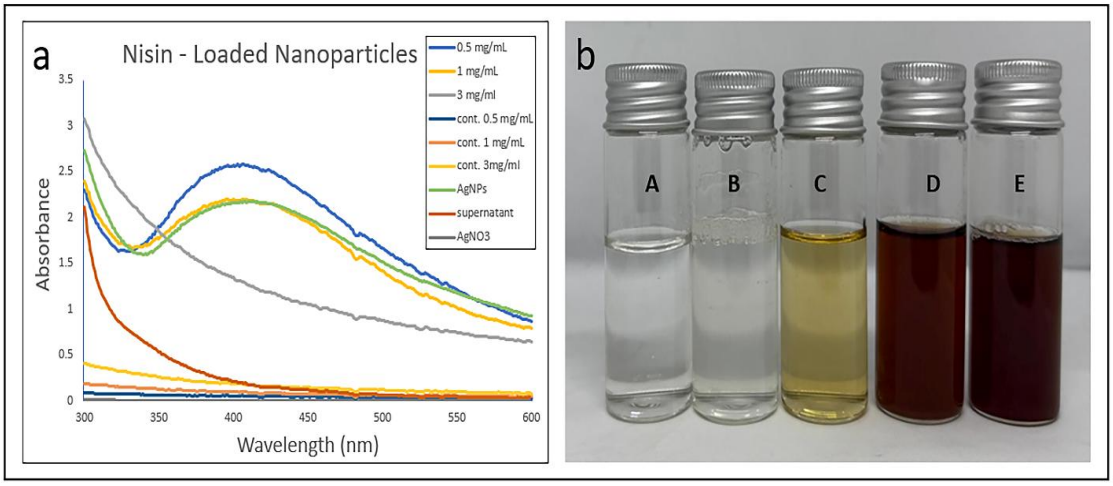


Fig. 2. (a) UV–vis spectra of nisin-loaded AgNPs, (b)(A) $AgNO_3$, (B) nisin, (C) *F. solani* supernatant, (D) AgNPs, and (E) N-AgNPs

shown in the size distribution histogram (Fig. 3A-b). The histogram of AgNPs shows high homogeneity and dispersion since most of the particles lie in the 6.4 –17.0 nm region. previous study [44] demonstrated that *C. acidovorans* yielded AgNPs with a smooth surface and spherical, oval, or irregular forms ranging from 6 to 53 nm.

TEM illustration (Fig. 3B-a) of N-AgNPs indicated a similar shape but with some higher particle size. Nisin loading expanded the distribution by surface adsorption and molecular interaction with AgNPs and raised the average particle size to 12.8 nm. As before reported, bio-conjugated nanoparticles with surface functionalization experience small size and heterogeneity changes [45,46]. whereas the sizes ranged from 7.9 nm to 18.1 nm (Fig. 3B-b). The histogram indicates a wider distribution than in simple AgNPs, which could be owing to the interaction between nisin and the nanoparticle surface, hence somewhat increasing the size [47].

SEM was used to investigate the morphology of NPs. SEM analysis was used to show that AgNPs and N-AgNPs were produced. An SEM study was done after the nanoparticle sample had been dried. A thin layer of the sample was made and examined. The microscopy images indicated that the nanoparticles were spread out evenly across the thin layer. However, a notable agglomeration of nanoparticles was observed, as shown in (Fig. 4A). Our approach produced a dense distribution of AgNPs and N-AgNPs with notable agglomeration using SEM examination. This observation is consistent with the results of [48]. who verified comparable nanoparticle characteristics using green banana peel extract. more monodispersed nanoparticles were observed [49]. which reduced the aggregation of the components in banana peel extract and therefore provided a lowered effective capping effect. Variations in aggregation degrees among studies could result from changes in synthesis conditions, including pH, temperature, and extract content, which influence the stabilization and dispersion of nanoparticles.

EDS was employed to analyze the chemical composition of the samples. EDS analysis of AgNPs indicated the presence of silver (Ag), shown by its

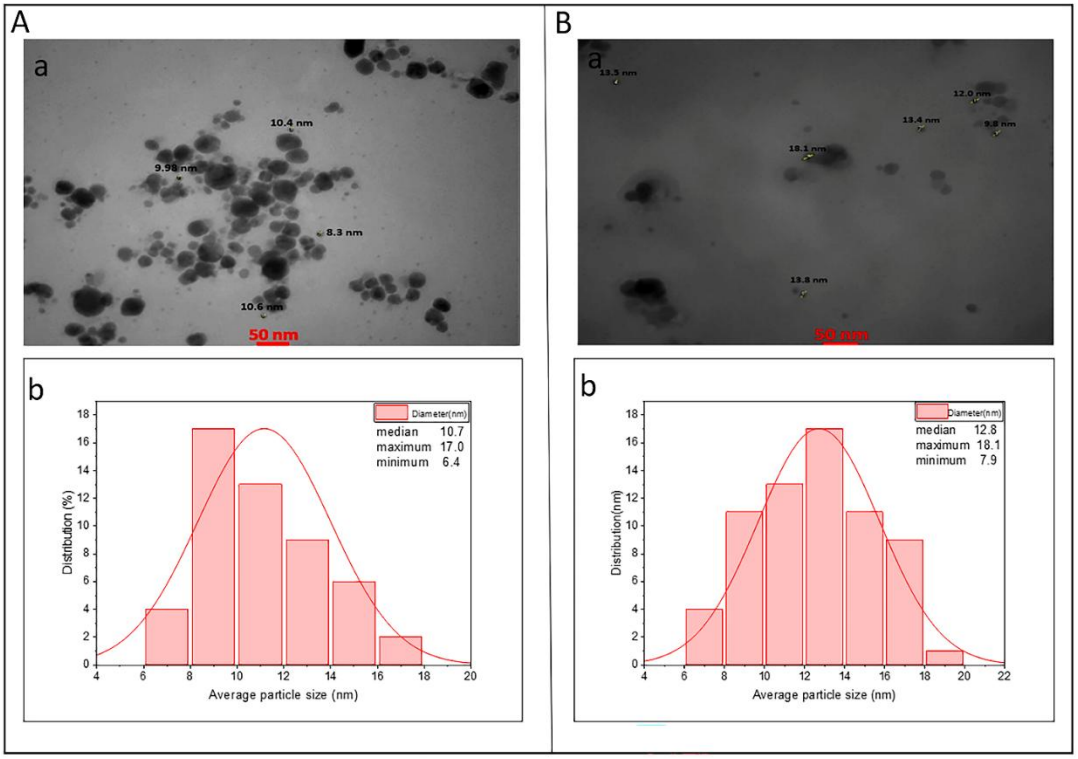


Fig. 3. (A-a) TEM photography of synthesized AgNPs, (b) size distribution histogram. (B-a) TEM image of N-AgNPs (b) histogram of size distribution. (at 50 nm scale).

characteristic peak at 3 keV, the peak position of the silver element. peaks at around 0.5 keV were also seen, suggesting the existence of oxygen and carbon, as reported in similar studies [50]. (Fig. 4B-a). Also, EDS analysis of N-AgNPs (Fig. 4B-b) approved the occurrence of silver and the organic elements incorporated with nitrogen and reveals the successful loading of nisin into the nanoparticles, the enhanced antibacterial action [51].

The crystalline structure of the synthesized NPs was analyzed using XRD . The XRD pattern exhibited characteristic diffraction peaks at 2θ values of 28.37°, 32.83°, 38.80°, 46.89°, 55.52°, 58.33°, and 77.70°. which can be index to plane (210), (122), (111), (200), (142), (241), and (311) planes of face-centered cubic (FCC) silver (Ag) (JCPDS card no. 04-0783) consistent with past studies on fungal-mediated synthesis [52-55]. As shown in Fig. 5A-a, this confirms the formation of crystalline AgNPs. The crystallite size is 9.23 nm, This value is calculated by employing the Debye-Scherrer equation to determine the (FWHM) of the peak that corresponds to 200 planes. Fig. 5A-b) shows the XRD pattern of the structure of N-AgNPs. Only three distinct peaks were shown at 2θ values $25.81^0$, $30.45^0$, and $50.78^0$, with a crystalline size of the particles increased to 14.29 nm upon loading with nisin, suggesting successful surface modification. This increase is following prior research, which demonstrated that the conjugation of peptides to AgNPs led to a quantifiable increase in particle size as a consequence of surface coating [56]. and a similar result was reported by [57]. showed that silver-nisin nanoparticles maintained their typical face-centered cubic silver crystalline structure, as seen by distinct XRD peaks at 2θ values of 38°, 44°, 64°, and 77°. This proves that nisin loading was effective without losing crystallinity.

AgNPs and N-AgNPs were confirmed in surface topography and shape using AFM imaging. It

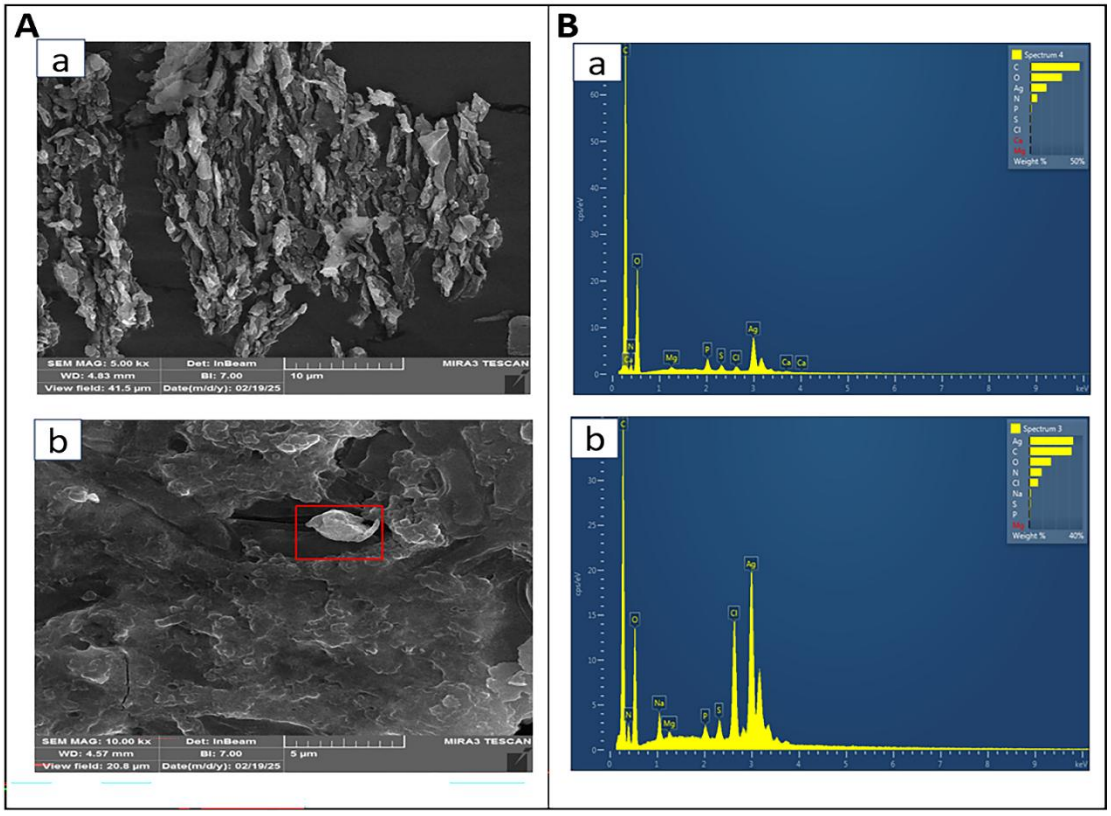


Fig. 4. (A)Scanning Electron Microscopy for :(a) synthesized AgNPs, (b) nisin-loaded nanoparticles, and (B)Energy dispersive X-ray spectrum of:(a) AgNPs, (b)N-AgNPs

was ascertained from the three-dimensional horizontal cross-section of both samples that the surface topography of the produced AgNPs and N-AgNPs were somewhat round in form (Fig. 5B.a-b). The N-AgNPs' surface seemed to be rather more textured, likely due to the presence of nisin on the surface of the nanoparticles [58] The functionalizing procedure involved in their synthesis [59].

FTIR spectroscopy is an effective technique to determine the bioactive groups of nanomaterials. In this study the FTIR spectra (Fig. 6A) shows the characteristic peaks that verify the existence of functional groups on the surface of AgNPs and N-AgNPs and free nisin. The O-H and N-H stretching vibrations were observed as a broad band around 3435–3422 $cm^{-1}$ and were indicative of hydroxyl groups and amines .The bands at 2957-2924 $cm^{-1}$ were assigned to C–H stretch, and are related to an aliphatic chain [60]. The proteins or peptides have an intense peak at approximately 1632 $cm^{-1}$ corresponding to C=O stretching (amide I band). The peaks at 1465$cm^{-1}$ belong to C-N stretching so indicating the presence of proteins or peptides involved in nanoparticle stabilization, respectively like what was found in consistent with past fungal-mediated synthesis studies [61,62]. , respectively, whereas those at 1112-1114 $cm^{-1}$ are due to C-O stretching. The Ag-O bond vibrations for peaks under 700 $cm^{-1}$ that form for the Ag nanoparticles can also be seen. As a whole, the FTIR spectra of nisin, AgNPs, and nisin-stabilized AgNPs were similar. (Fig. 6A) illustrated that nisin was successfully loaded onto AgNPs. Comparatively the FTIR spectra show the common peaks of relevant to AgNPs , N-AgNPs , and free nisin , especially those for O-H/N-H stretching 3430 $cm^{-1}$ , C-H stretching 2957–2924 $cm^{-1}$ , and the amid I band 1632 $cm^{-1}$indicating the coexistence of biomolecules on the nanoparticle surface. Peaks attributed to C-O stretching at 1112–1114 $cm^{-1}$ and Ag–O vibrations below 700 $cm^{-1}$ were also observed . these spectral feature, specially amid I and O-H/N-H bands are commonly reported in previous study in biosynthesized AgNPs and reflected by capping peptide and protein . similarities between the spectra of nisin and nanoparticles indicated the effective stabilization and interaction of AgNPs by nisin.

The zeta potential value confirms that AgNP is moderately stable even further. The AgNPs were negatively charged in the dispersed media,

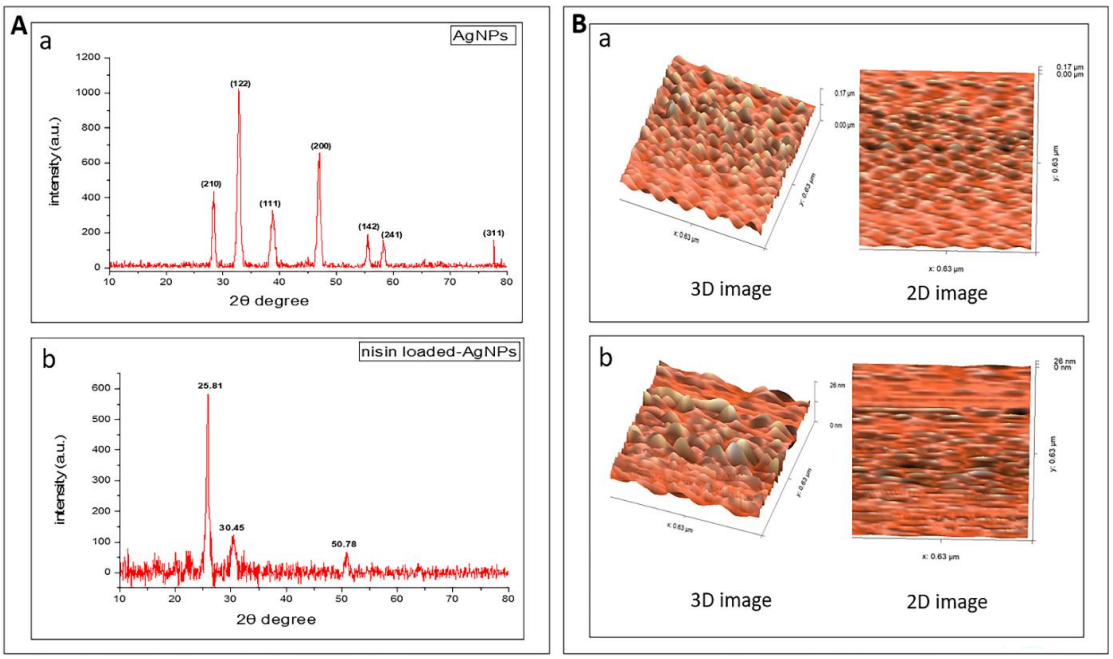


Fig. 5. (A) XRD pattern for biosynthesized (a) AgNPs, (b) nisin-loaded AgNPs. (B) AFM image of synthesized AgNPs using *F. solani* (a) 3D image and 2D image of AgNPs, (b)AFM image of N-AgNPs (a) 3D image and 2D image of N-AgNPs

hence, the resulting value of -3.7 mV (Fig. 6B-a). The results showed that the particles repelled one another, thereby preventing aggregation. While nisin was loaded onto AgNPs, enhanced stability was observed. while free nisin was added dropwise at a low concentration to the NPs solution, more nanoparticles with the same charges were wrapped by negatively charged molecules as confirmed by the zeta potential of –38.4 mV this number shows a stable colloidal solution of N-AgNPs. the value reveals that the generated nanoparticles have well-dispersed electrostatic stability in suspension (Fig. 6B-b). This improvement corresponds with those [63]. who attributed the higher stability to the capping effect of nisin's amine and amide groups and found that nisin-capped AgNPs had zeta potential values of –23.2 mV and –27.0 mV. Similarly, [64]. found that nisin added to AgNPs raised the zeta potential values of the bioconjugates, enhancing stability and antibacterial action.

*Molecular identification of bacteria*

This study identified bacterial isolates using BD Phoenix and 16S rRNA gene sequencing. The automated phenotypic identification system BD Phoenix identified the clinical isolates as *E. coli, A. baumannii,* and *S. aureus*, common hospital organisms. The PCR products were sequenced, and the sequences were aligned to sequences representing known bacteria available on the National Center for Biotechnology Information (NCBI) database. The bacterial isolates were identified as *E. coli, A. baumannii*, and *S. aureus,* and the DNA sequence of the 16s rRNA gene of each of the isolates was submitted to the BANKIT, and gene bank accession numbers were assigned to all of the 16s rRNA sequences. Accession numbers were assigned for each sequence as follows: *E. coli* strain AD2 *(*PV596248.1), *A. baumannii* strain AD3 *(PV596249.1),* and *S. aureus* strain AD1 *(PV596247.1)*. The phylogenetic tree of isolates was constructed based on the 16S rRNA gene sequence. (Fig. 7) A newly isolated of *E. coli* strain AD2 formed a monophyletic group with other *E. coli* strains such as strain T18-6-1 (accession numbers: PQ097308.1), which was isolated from Japan, and strain DSM 112117 (accession numbers:

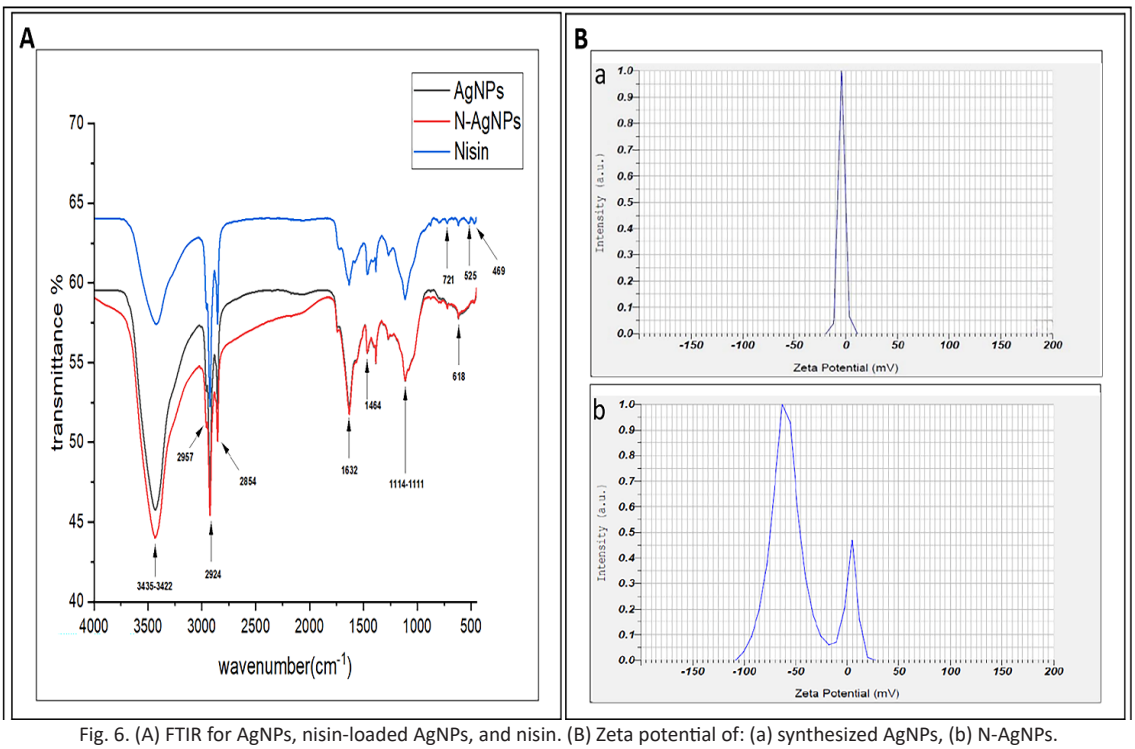


Fig. 6. (A) FTIR for AgNPs, nisin-loaded AgNPs, and nisin. (B) Zeta potential of: (a) synthesized AgNPs, (b) N-AgNPs.

OM658577.1) isolated from Germany, which shows a common ancestral lineage. Similarly, a new *A. baumannii* isolated (AD3) clustered withing strongly supported monophyletic clade with strain C9 (accession numbers: MK070057.1) isolated from Washington DC, strain M.pstv.34.1(accession numbers: KM108526.1) isolated from France, and strain GPUL16(accession numbers: MF398381.1) isolated from India. In contrast, the newly isolated *S. aureus* strain (AD1) formed only a monophyletic group with strain AHL21(accession numbers: MN067694.1), which was previously isolated from Iraq.

*Antibacterial activity assay*

Disc diffusion was used to assess the antibacterial activity of AgNPs and N-AgNPs against clinically isolated bacterial strains such as *E. coli, A. baumannii, and S. aureus.* We depicted that N-AgNPs have a larger zone of inhibition compared to AgNPs alone. At 4 mg/ml concentration, AgNPs produced an 11 mm inhibition zone for Gram-negative bacteria, including *E. coli* , but this zone expanded to 14 mm when N-AgNPs were used, which demonstrated a 3 mm improvement. *A. baumannii.* AgNPs produced a 9.66 mm inhibitory zone, N-AgNPs raised this value to 12.33 mm, so improving by 2.67 mm. Regarding Gram-positive bacteria like *S. aureus*, the inhibitory zone grew from 8 mm with AgNPs to 9.66 mm with N-AgNPs, increasing the difference by 1.66 mm, as shown in (Table 1). The inhibition zone measured for nisin alone was 6.1mm for *E. coli*, 6.6mm for A. *Baumannii* and, 7 mm for S. *Aureus.* Indicates a synergistic effect when combined with AgNPs. A naturally occurring antimicrobial peptide, nisin may increase the bactericidal effect of AgNPs when combined. AgNPs and antimicrobials boost antibacterial efficacy. according to other studies, AgNPs alone did not raise *P. aeruginosa* inhibition zones [65,66] discovered that they have a greater effect when nisin is loaded onto AgNPs against the studied bacteria. Nisin-conjugated zinc oxide nanoparticles have enhanced antibacterial activity against *E. coli* and *S. aureus* [13]. This enhanced impact results from nisin's binding to lipid II, a necessary component of bacterial cell wall formation, and disturbance of membrane

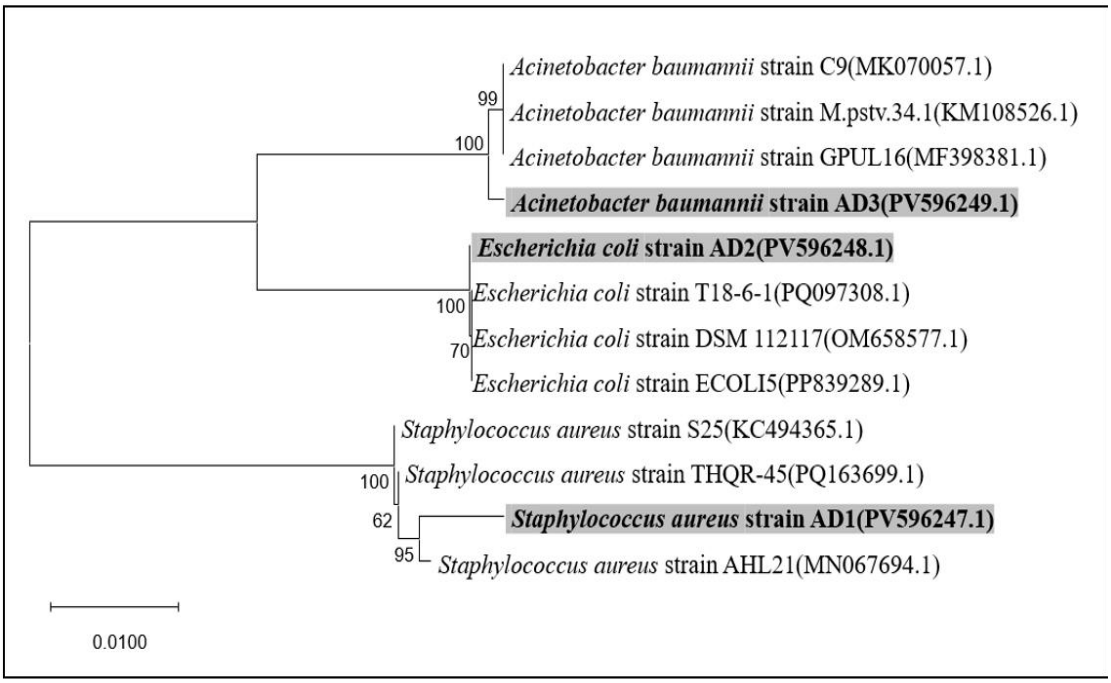


Fig. 7. illustrates the phylogenetic tree of *Acinetobacter baumannii* strain AD3, *Escherichia coli* strain AD2, and *Staphylococcus aureus* strain AD1 as determined by the 16s rRNA gene sequence. The ClustalX program was employed to align DNA sequences, and the MEGA 12 tree-building program was employed to construct the tree using the neighbor-joining method. The bootstrapped was performed with 1,000 replicate trials.

integrity by creating holes, therefore promoting the increased antibacterial activity of AgNPs [67]. Published similar results showing enhanced activity of biogenic AgNPs mixed with nisin; Elsherif and his friends [68]. revealed that nisin nanoparticles had higher effects against *S. aureus* and *E. coli* O157:H7.

Table 2 confirms that N-AgNPs reveal greater antibacterial activity than AgNPs alone. As a lower concentration is required to inhibit the bacterial growth for Gram-negative bacteria, Results showed that *E. coli* showed a two-fold reduction in MIC test (0.25mg/ml for N-AgNPs vs. 0.50 mg/ml for AgNPs ), At the same time, bioconjugation of AgNPs with nisin resulted in a significant reduction of MIC values. respectively, for Gram-positive bacteria *S. aureus*. These findings are consistent with what other research have shown. For example, [69] found that silver-nisin conjugates had lower MICs (4 µg/ml for *S. aureus* and 2 µg/ml for *E. coli*). but *A. baumannii,* showed no difference in MIC (at 0.5 mg/ml for AgNPs and N-AgNPs) (Table 2). regardless of how nisin is conjugated. Some research [70]. on the other hand, say that N-AgNP conjugates work better against *A. baumannii*, with MICs in the 52–125 µg/ml range. N-AgNPs showed considerable reductions in MIC values for *E. coli* and *S. aureus* after bioconjugation with nisin ($p < 0.05$), suggesting improved antibacterial action compared to AgNPs alone. Nisin conjugation did not improve antibacterial activity against *A. baumannii*.

*Antibiofilm Inhibition Assay*

Various concentrations (1, 0.5, 0.25, 0.125, and 0.06 mg/ml) of biosynthesized AgNPs and N-AgNPs were utilized to examine their effectiveness in preventing biofilm formation in clinically isolated bacteria this study, AgNPs and N-AgNPs greatly inhibited the formation of biofilm. The synergistic activity of nisin and AgNPs is responsible for the increased effectiveness of N-AgNPs, especially at lower doses. AgNPs reduced biofilm at 0.5 mg/ml in *E. coli*, but N-AgNPs were completely

Table 1. Antibacterial activity of AgNPs and N-AgNPs against clinically isolated bacteria

| | Microorganisms | | | | | |
|---|---|---|---|---|---|---|
| | *Escherichia coli* | | *Acinetobacter baumannii* | | *Staphylococcus Aureus* | |
| Concentrations (mg/ml) | Zone Diameter (mm) AgNPs | N-AgNPs | Zone Diameter (mm) AgNPs | N-AgNPs | Zone Diameter (mm) AgNPs | N-AgNPs |
| 1 | $7.66^{a}$ ±0.4 | $9.3^{a}$ ±0.5 | $6.8^{a}$ ±0.6 | $7.3^{a}$ ±0.4 | $5.8^{a}$ ±0.2 | $7.5^{a}$ ±0.4 |
| 2 | $9.3^{ab}$ ±0.4 | $10.5^{b}$ ±0.4 | $8.0^{b}$ ±0.4 | $8.8^{b}$ ±0.2 | $7.3^{a}$ ±0.6 | $8.7^{ab}$ ±0.9 |
| 3 | $10.2^{c}$ ±0.6 | $11.8^{c}$ ±0.2 | $8.2^{b}$ ±0.2 | $10.3^{c}$ ± 0.4 | $8.3^{a}$ ±0.4 | $9.0^{ab}$ ±0.8 |
| 4 | $11.0^{d}$ ±0.8 | $14.3^{d}$ ±0.9 | $9.7^{c}$ ± 0.4 | $12.3^{d}$ ±0.5 | $8.0^{b}$ ±0.4 | $9.7^{b}$ ±0.4 |

Table 2. Minimum inhibitory concentration of AgNPs and N-AgNPs against Gram-negative and Gram-positive bacteria.

| Microorganisms | MIC of AgNPs (mg/ml) | MIC of N-AgNPs (mg/ml) |
|---|---|---|
| *Escherichia coli* | 0.50 ±0.04 | 0.25 ±0.06 |
| *Acinetobacter baumannii* | 0.50 ±0.04 | 0.50 ±0.10 |
| *Staphylococcus Aureus* | 0.25 ±0.03 | 0.125 ±0.03 |

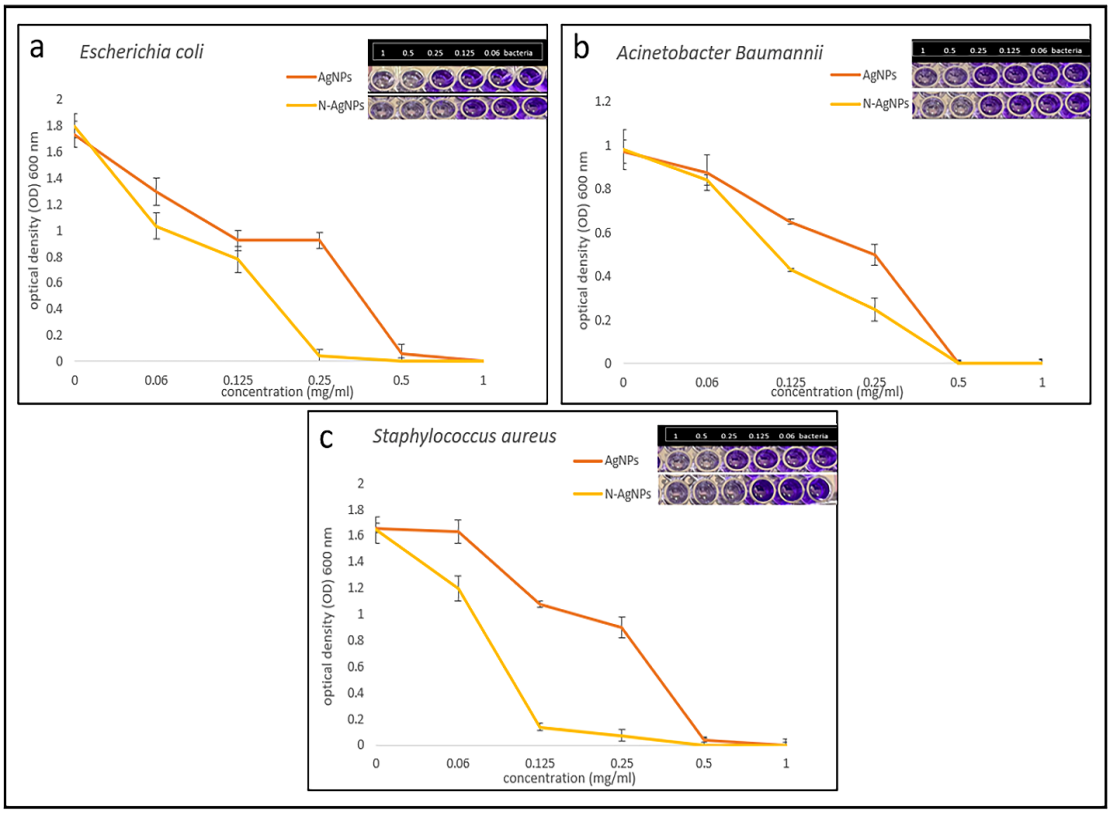


Fig. 8. Antibiofilm of AgNPs and N-AgNPs against clinically isolated bacteria using different concentrations (a) *Escherichia coli*, (b) *Acinetobacter baumannii,* and (c) *Staphylococcus aureus.*

inhibited at 0.25 mg/ml, thus demonstrating the capacity of nisin to increase nanoparticle penetration Similar findings were reported by [71]. who observed that nisin-functionalized nanoparticles exhibited greater antimicrobial effects against Gram-negative pathogens due to improved delivery and stability. Likewise, at 0.5 mg/ml AgNPs and N-AgNPs, reduced biofilm in *A. baumannii*, suggesting a cooperative action against this pathogen [72]. Notably, N-AgNPs were strongly efficacious against *S. aureus*, with complete biofilm removal noted at 0.125 mg/ml. These results reinforce the greater susceptibility of Gram-positive bacteria to nisin–based treatments, possibly because of its thick peptidoglycan layer, which could be efficiently targeted by the pore–formation capability of nisin [73]. In contrast, the same AgNPs alone at higher concentrations result in only partial inhibition. A similar phenomenon was reported by [74]. which observed that the bioactivity of NPs after being modified with antimicrobial agents is also improved, leading to a greater substance efficacy of anti-biofilm activity against *S. aureus*. The difference between the two statements was statistically significant ($P$<0.05) at all concentrations. The results suggest that loading nisin onto AgNPs increases their biofilm-disrupting potential against clinically isolated bacteria (Fig. 8).

## CONCLUSION

This study successfully highlights the bio-synthesized AgNPs using fungal supernatant and nisin loaded onto AgNPs. Characterization techniques include UV-vis spectroscopy, TEM, SEM, EDS, XRD, AFM, FTIR, and Zeta potential, verified structural integrity, production, and effective conjugation of nisin onto AgNPs, with improved colloidal stability and greater particle sizes. The results of antibacterial and antibiofilm experiments demonstrated that N-AgNPs exhibited significantly enhanced antimicrobial and antibiofilm activity against clinically isolated Gram-negative and Gram-positive bacteria.

compare to AgNPs alone. These findings highlight the efficacy of nisin-functionalized AgNPs as a viable antibacterial and antibiofilm agent against clinically isolated pathogenic bacteria.

## ACKNOWLEDGMENTS

The authors would like to thank the research center of Charmo University for providing laboratory equipment and support throughout this study, special thanks extended to professor Dr. Haider Mousa Hamzah for valuable assistance and guidance during this research, and miss Payman M. Mohamed salih for her helpful support during the laboratory work. Also We also thank the head of the Medical Laboratory Science Department for continuous support.

## CONFLICT OF INTEREST

The authors declare that there is no conflict of interest regarding the publication of this manuscript.

## REFERENCES

1. Zhang F, Cheng W. The Mechanism of Bacterial Resistance and Potential Bacteriostatic Strategies. Antibiotics. 2022;11(9):1215.
2. Mancuso G, Midiri A, Gerace E, Biondo C. Bacterial Antibiotic Resistance: The Most Critical Pathogens. Pathogens. 2021;10(10):1310.
3. Fattah B, Arif H, Hamzah H. Antimicrobial and Antibiofilm Activity of Biosynthesized Silver Nanoparticles Against Beta-lactamase-Resistant Enterococcus faecalis. Applied Biochemistry and Biotechnology. 2022;194(5):2036-2046.
4. Rather MA, Gupta K, Mandal M. Microbial biofilm: formation, architecture, antibiotic resistance, and control strategies. Braz J Microbiol. 2021;52(4):1701-1718.
5. Franci G, Falanga A, Galdiero S, Palomba L, Rai M, Morelli G, et al. Silver Nanoparticles as Potential Antibacterial Agents. Molecules. 2015;20(5):8856-8874.
6. Rai M, Yadav A, Gade A. Silver nanoparticles as a new generation of antimicrobials. Biotechnol Adv. 2009;27(1):76-83.
7. Zhang X-F, Liu Z-G, Shen W, Gurunathan S. Silver Nanoparticles: Synthesis, Characterization, Properties, Applications, and Therapeutic Approaches. Int J Mol Sci. 2016;17(9):1534.
8. Bakhtyar R, Tofiq R, Hamzah H, Qurbani K. Fabricated Fusarium species-mediated nanoparticles against Gram-negative pathogen (Review). World Academy of Sciences Journal. 2024;7(1).
9. Darwish RM, Salama AH. Study the Effect of Conjugate Novel Ultra-Short Antimicrobial Peptide with Silver Nanoparticles against Methicillin Resistant S. aureus and ESBL E. coli. Antibiotics. 2022;11(8):1024.
10. Zharkova MS, Golubeva OY, Orlov DS, Vladimirova EV, Dmitriev AV, Tossi A, et al. Silver Nanoparticles Functionalized With Antimicrobial Polypeptides: Benefits and Possible Pitfalls of a Novel Anti-infective Tool. Front Microbiol. 2021;12.
11. Krivorotova T, Cirkovas A, Maciulyte S, Staneviciene R, Budriene S, Serviene E, et al. Nisin-loaded pectin nanoparticles for food preservation. Food Hydrocolloids. 2016;54:49-56.
12. Zimet P, Valadez R, Raffaelli S, Estevez MB, Pardo H, Alborés S. Biogenic Silver Nanoparticles Conjugated with Nisin: Improving the Antimicrobial and Antibiofilm Properties of Nanomaterials. Chemistry (Easton). 2021;3(4):1271-1285.
13. Hamk M, Avcı A. One-pot approach biosynthesis of nisin-conjugated zinc oxide nanoparticles using Bacillus subtilis ZBP4 with improved antibacterial activity. Biomass Conversion and Biorefinery. 2024;15(7):9941-9949.
14. Panina I, Krylov N, Nolde D, Efremov R, Chugunov A. Environmental and dynamic effects explain how nisin captures membrane-bound lipid II. Sci Rep. 2020;10(1).
15. Tang CY, Yang Z. Transmission Electron Microscopy (TEM). Membrane Characterization: Elsevier; 2017. p. 145-159.
16. Karak N. Silver Nanomaterials and Their Polymer Nanocomposites. Nanomaterials and Polymer Nanocomposites: Elsevier; 2019. p. 47-89.
17. Madhavi J. Comparison of average crystallite size by X-ray peak broadening and Williamson–Hall and size–strain plots for VO2+ doped ZnS/CdS composite nanopowder. SN Applied Sciences. 2019;1(11).
18. Rabiei M, Palevicius A, Monshi A, Nasiri S, Vilkauskas A, Janusas G. Comparing Methods for Calculating Nano Crystal Size of Natural Hydroxyapatite Using X-Ray Diffraction. Nanomaterials. 2020;10(9):1627.
19. Khan MK, Wang QY, Fitzpatrick ME. Atomic force microscopy (AFM) for materials characterization. Materials Characterization Using Nondestructive Evaluation (NDE) Methods: Elsevier; 2016. p. 1-16.
20. Fattah B, Arif H, Hamzah H. In vitro biofabrication of silver nanoparticles: Optimization, characterization, and activity against beta-lactamases-resistant Enterococcus faecalis. Springer Science and Business Media LLC; 2021.
21. Onugwu AL, Nwagwu CS, Onugwu OS, Echezona AC, Agbo CP, Ihim SA, et al. Nanotechnology based drug delivery systems for the treatment of anterior segment eye diseases. Journal of Controlled Release. 2023;354:465-488.
22. Carroll KC, Borek AP, Burger C, Glanz B, Bhally H, Henciak S, et al. Evaluation of the BD Phoenix Automated Microbiology System for Identification and Antimicrobial Susceptibility Testing of Staphylococci and Enterococci. J Clin Microbiol. 2006;44(6):2072-2077.
23. Mohamedsalih P, Sabir D. Antimicrobial Activity of Silver Nanoparticles with Antibiotics Against Clinically Isolated Acinetobacter baumannii. passer. 2020;2:51-56.
24. Satokari RM, Vaughan EE, Akkermans ADL, Saarela M, de Vos WM. Bifidobacterial Diversity in Human Feces Detected by Genus-Specific PCR and Denaturing Gradient Gel Electrophoresis. Applied and Environmental Microbiology. 2001;67(2):504-513.
25. Chong CS, Sabir DK, Lorenz A, Bontemps C, Andeer P, Stahl DA, et al. Analysis of the xplAB -Containing Gene Cluster Involved in the Bacterial Degradation of the Explosive Hexahydro-1,3,5-Trinitro-1,3,5-Triazine. Applied and Environmental Microbiology. 2014;80(21):6601-6610.
26. Sievers F, Wilm A, Dineen D, Gibson TJ, Karplus K, Li W, et al. Fast, scalable generation of high-quality protein multiple sequence alignments using Clustal Omega. Mol Syst Biol. 2011;7(1).

27. Kumar S, Stecher G, Li M, Knyaz C, Tamura K. MEGA X: Molecular Evolutionary Genetics Analysis across Computing Platforms. Molecular Biology and Evolution. 2018;35(6):1547-1549.
28. Kourmouli A, Valenti M, van Rijn E, Beaumont HJE, Kalantzi O-I, Schmidt-Ott A, et al. Can disc diffusion susceptibility tests assess the antimicrobial activity of engineered nanoparticles? J Nanopart Res. 2018;20(3).
29. Singh P, Pandit S, Beshay M, Mokkapati VRSS, Garnaes J, Olsson ME, et al. Anti-biofilm effects of gold and silver nanoparticles synthesized by the Rhodiola rosea rhizome extracts. Artificial Cells, Nanomedicine, and Biotechnology. 2018;46(sup3):886-899.
30. Sogra Fathima B, Balakrishnan RM. Biosynthesis and optimization of silver nanoparticles by endophytic fungus Fusarium solani. Mater Lett. 2014;132:428-431.
31. Birla SS, Gaikwad SC, Gade AK, Rai MK. Rapid Synthesis of Silver Nanoparticles from Fusarium oxysporum by Optimizing Physicocultural Conditions. The Scientific World Journal. 2013;2013(1).
32. Kathiravan V, Ravi S, Ashokkumar S, Velmurugan S, Elumalai K, Khatiwada CP. Green synthesis of silver nanoparticles using Croton sparsiflorus morong leaf extract and their antibacterial and antifungal activities. Spectrochimica Acta Part A: Molecular and Biomolecular Spectroscopy. 2015;139:200-205.
33. Adebayo-Tayo B, Salaam A, Ajibade A. Green synthesis of silver nanoparticle using Oscillatoria sp. extract, its antibacterial, antibiofilm potential and cytotoxicity activity. Heliyon. 2019;5(10):e02502.
34. Vigneshwaran N, Ashtaputre NM, Varadarajan PV, Nachane RP, Paralikar KM, Balasubramanya RH. Biological synthesis of silver nanoparticles using the fungus Aspergillus flavus. Mater Lett. 2007;61(6):1413-1418.
35. Ingle A, Rai M, Gade A, Bawaskar M. Fusarium solani: a novel biological agent for the extracellular synthesis of silver nanoparticles. J Nanopart Res. 2008;11(8):2079-2085.
36. Othman AM, Elsayed MA, Al-Balakocy NG, Hassan MM, Elshafei AM. Biosynthesis and characterization of silver nanoparticles induced by fungal proteins and its application in different biological activities. Journal of Genetic Engineering and Biotechnology. 2019;17(1):8.
37. Yazdi M, Yousefvand A, Hosseini HM, Mirhosseini SA. Green Synthesis of Silver Nanoparticles Using Nisin and its Antibacterial Activity against Pseudomonas aeruginosa. Advanced Biomedical Research. 2022;11(1):56.
38. Iravani S. Green synthesis of metal nanoparticles using plants. Green Chem. 2011;13(10):2638.
39. Palepu NR, Richard Premkumar J, Verma AK, Bhattacharjee K, Joshi SR, Forbes S, et al. Antibacterial, in vitro antitumor activity and structural studies of rhodium and iridium complexes featuring the two positional isomers of pyridine carbaldehyde picolinic hydrazone ligand. Arabian Journal of Chemistry. 2018;11(5):714-728.
40. Durán N, Marcato PD, Alves OL, De Souza GIH, Esposito E. Mechanistic aspects of biosynthesis of silver nanoparticles by several Fusarium oxysporum strains. Journal of Nanobiotechnology. 2005;3(1).
41. Jeschek M, Panke S, Ward TR. Artificial Metalloenzymes on the Verge of New-to-Nature Metabolism. Trends Biotechnol. 2018;36(1):60-72.
42. Ahmed S, Saifullah, Ahmad M, Swami BL, Ikram S. Green synthesis of silver nanoparticles using Azadirachta indica aqueous leaf extract. Journal of Radiation Research and Applied Sciences. 2016;9(1):1-7.
43. Othman AM, Elsayed MA, Al-Balakocy NG, Hassan MM, Elshafei AM. Correction to: Biosynthesis and characterization of silver nanoparticles induced by fungal proteins and its application in different biological activities. Journal of Genetic Engineering and Biotechnology. 2020;18(1):7.
44. Rudakiya DM, Pawar K. Bactericidal potential of silver nanoparticles synthesized using cell-free extract of Comamonas acidovorans: in vitro and in silico approaches. 3 Biotech. 2017;7(2).
45. Bernela M, Kaur P, Chopra M, Thakur R. Synthesis, characterization of nisin loaded alginate–chitosan–pluronic composite nanoparticles and evaluation against microbes. LWT - Food Science and Technology. 2014;59(2):1093-1099.
46. Arakha M, Borah SM, Saleem M, Jha AN, Jha S. Interfacial assembly at silver nanoparticle enhances the antibacterial efficacy of nisin. Free Radical Biology and Medicine. 2016;101:434-445.
47. Arakha M, Saleem M, Mallick BC, Jha S. The effects of interfacial potential on antimicrobial propensity of ZnO nanoparticle. Sci Rep. 2015;5(1).
48. Ohiduzzaman M, Khan MNI, Khan KA, Paul B. Biosynthesis and characterizations of silver nanoparticles by using green banana peel extract: Evaluation of their antibacterial and electrical performances. Heliyon. 2024;10(10):e31140.
49. Ibrahim HMM. Green synthesis and characterization of silver nanoparticles using banana peel extract and their antimicrobial activity against representative microorganisms. Journal of Radiation Research and Applied Sciences. 2015;8(3):265-275.
50. Singh H, Du J, Yi T-H. KinneretiaTHG-SQI4 mediated biosynthesis of silver nanoparticles and its antimicrobial efficacy. Artificial Cells, Nanomedicine, and Biotechnology. 2016;45(3):602-608.
51. Behnia B, Aali Anvari A, Safardoust-Hojaghan H, Salavati-Niasari M. Positive effects of novel nano-zirconia on flexural and compressive strength of Portland cement paste. Polyhedron. 2020;177:114317.
52. Shende S, Gade A, Rai M. Large-scale synthesis and antibacterial activity of fungal-derived silver nanoparticles. Environ Chem Lett. 2016;15(3):427-434.
53. Meng Y. A Sustainable Approach to Fabricating Ag Nanoparticles/PVA Hybrid Nanofiber and Its Catalytic Activity. Nanomaterials. 2015;5(2):1124-1135.
54. Vanaja M, Annadurai G. Coleus aromaticus leaf extract mediated synthesis of silver nanoparticles and its bactericidal activity. Applied Nanoscience. 2012;3(3):217-223.
55. Wang D, Xue B, Wang L, Zhang Y, Liu L, Zhou Y. Fungus-mediated green synthesis of nano-silver using Aspergillus sydowii and its antifungal/antiproliferative activities. Sci Rep. 2021;11(1).
56. Nagaonkar D, Rai M. Sequentially Reduced Biogenic Silver-gold Nanoparticles With Enhanced Antimicrobial Potential Over Silver And Gold Monometallic Nanoparticles. Advanced Materials Letters. 2015;6(4):334-341.
57. Zhao X, Kuipers OP. Synthesis of silver-nisin nanoparticles with low cytotoxicity as antimicrobials against biofilm-forming pathogens. Colloids Surf B Biointerfaces. 2021;206:111965.
58. Pandit R, Rai M, Santos CA. Enhanced antimicrobial activity

of the food-protecting nisin peptide by bioconjugation with silver nanoparticles. Environ Chem Lett. 2017;15(3):443-452.
59. Azevedo N, de Medeiros A, da Silva G, Brito M, Faria J, Delite F, et al. Biocorona Formation and Hemolytic Effects of Graphene Oxide-Silver Nanoparticles. J Braz Chem Soc. 2024.
60. Mohammad-Salehi H, Hamadanian M, Safardoust-Hojaghan H. Visible-Light Induced Photodegradation of Methyl Orange via Palladium Nanoparticles Anchored to Chrome and Nitrogen Doped $TiO_2$ Nanoparticles. Journal of Inorganic and Organometallic Polymers and Materials. 2019;29(5):1457-1465.
61. Roy N, Gaur A, Jain A, Bhattacharya S, Rani V. Green synthesis of silver nanoparticles: An approach to overcome toxicity. Environmental Toxicology and Pharmacology. 2013;36(3):807-812.
62. Anandalakshmi K, Venugobal J, Ramasamy V. Characterization of silver nanoparticles by green synthesis method using Pedalium murex leaf extract and their antibacterial activity. Applied Nanoscience. 2015;6(3):399-408.
63. Belén Estevez M, Raffaelli S, Mitchell S, Faccio R, Alborés S. Biogenic silver nanoparticles against Escherichia coli planktonic and biofilm cells. American Chemical Society (ACS); 2020.
64. Senthilkumar P, Rashmitha S, Veera P, Ignatious C, SaiPriya C, Samrot A. Antibacterial Activity of Neem Extract and its Green Synthesized Silver Nanoparticles against Pseudomonas aeruginosa. Journal of Pure and Applied Microbiology. 2018;12(2):969-974.
65. Bose D, Chatterjee S. Biogenic synthesis of silver nanoparticles using guava (Psidium guajava) leaf extract and its antibacterial activity against Pseudomonas aeruginosa. Applied Nanoscience. 2015;6(6):895-901.
66. S H, V M, S A. Biosynthesis of Zinc Oxide Nanoparticles Using Bacillus Species Potentiates Anticancer and Antimicrobial Activity. International Journal of Trend in Scientific Research and Development. 2018;Volume-2(Issue-5):1796-1802.
67. Safardoust-Hojaghan H, Shakouri-Arani M, Salavati-Niasari M. A facile and reliable route to prepare of lead sulfate nanostructures in the presence of a new sulfur source. Journal of Materials Science: Materials in Electronics. 2014;26(3):1518-1524.
68. Elsherif WM, Hassanien AA, Zayed GM, Kamal SM. Natural approach of using nisin and its nanoform as food bio-preservatives against methicillin resistant Staphylococcus aureus and E.coli O157:H7 in yoghurt. BMC Vet Res. 2024;20(1).
69. Tavares TD, Ribeiro ARM, Silva C, Antunes JC, Felgueiras HP. Combinatory effect of nisin antimicrobial peptide with bioactive molecules: A review. J Drug Deliv Sci Technol. 2024;91:105246.
70. Ahmed MS, Abdulrahman ZFA, Taha ZMA. The effect of silver nanoparticles on the antimicrobial activity of cloned nisin against extensively drug-resistant Acinetobacter baumannii". Journal of Infection and Public Health. 2024;17(9):102501.
71. Rashki S, Dawi EA, Zilaei MR, Safardoust-Hojaghan H, Ghanbari M, Ryadh A, et al. ZnO/chitosan nanocomposites as a new approach for delivery LL37 and evaluation of the inhibitory effects against biofilm-producing Methicillin-resistant Staphylococcus aureus isolated from clinical samples. Int J Biol Macromol. 2023;253:127583.
72. Yadav A, Rai M. Phytosynthesis of Silver Nanoparticles and Their Role as Antimicrobials. Synthesis and Applications of Nanoparticles: Springer Nature Singapore; 2022. p. 357-369.
73. Hassanpour M, Salavati-Niasari M, Safardoust-Hojaghan H. Sol-gel synthesis and characterization of $Co_3O4/CeO_2$ nanocomposites and its application for photocatalytic discoloration of organic dye from aqueous solutions. Environmental Science and Pollution Research. 2020;28(6):7001-7015.
74. Hajipour MJ, Fromm KM, Akbar Ashkarran A, Jimenez de Aberasturi D, Larramendi IRd, Rojo T, et al. Antibacterial properties of nanoparticles. Trends Biotechnol. 2012;30(10):499-511.